



# Development and Characterization of $\text{SiC}/\text{MoSi}_2\text{-Si}_3\text{N}_{4(p)}$ Hybrid Composites

Mohan G. Hebsur  
Ohio Aerospace Institute, Brook Park, Ohio

Prepared under Cooperative Agreement NCC3-637

National Aeronautics and  
Space Administration

Lewis Research Center

## Acknowledgments

The author would like to acknowledge financial support from the Office of the Naval Research, (A.K. Vasudevan ), NASA-LeRC (M.V. Nathal), and Pratt & Whitney Aircraft, West Palm Beach, FL (W. Pospisil).

This report is a formal draft or working paper, intended to solicit comments and ideas from a technical peer group.

This report contains preliminary findings, subject to revision as analysis proceeds.

Trade names or manufacturers' names are used in this report for identification only. This usage does not constitute an official endorsement, either expressed or implied, by the National Aeronautics and Space Administration.

Available from

NASA Center for Aerospace Information  
7121 Standard Drive  
Hanover, MD 21076  
Price Code: A03

National Technical Information Service  
5285 Port Royal Road  
Springfield, VA 22100  
Price Code: A03

# **DEVELOPMENT AND CHARACTERIZATION OF SiC<sub>(f)</sub>/MoSi<sub>2</sub>-Si<sub>3</sub>N<sub>4(p)</sub> HYBRID COMPOSITES**

**Mohan G. Hebsur  
NASA Lewis Research Center  
21000 Brookpark Road  
Cleveland, Ohio 44135**

## **ABSTRACT**

Intermetallic compound MoSi<sub>2</sub> has long been known as a high temperature material that has excellent oxidation resistance and electrical/thermal conductivity. Also its low cost, high melting point (2023 °C), relatively low density (6.2 g/cm<sup>3</sup> versus 9 g/cm<sup>3</sup> for current engine materials), and ease of machining, make it an attractive structural material. However, the use of MoSi<sub>2</sub> has been hindered due to its poor toughness at low temperatures, poor creep resistance at high temperatures, and accelerated oxidation (also known as 'pest' oxidation) at temperatures between approximately 450 and 550 °C. Continuous fiber reinforcing is very effective means of improving both toughness and strength. Unfortunately, MoSi<sub>2</sub> has a relatively high coefficient of thermal expansion (CTE) compared to potential reinforcing fibers such as SiC. The large CTE mismatch between the fiber and the matrix resulted in severe matrix cracking during thermal cycling.

Addition of about 30 to 50 vol % of Si<sub>3</sub>N<sub>4</sub> particulate to MoSi<sub>2</sub> improved resistance to low temperature accelerated oxidation by forming a Si<sub>2</sub>ON<sub>2</sub> protective scale and thereby eliminating catastrophic 'pest failure'. The Si<sub>3</sub>N<sub>4</sub> addition also improved the high temperature creep strength by nearly five orders of magnitude, doubled the room temperature toughness and significantly lowered the CTE of the MoSi<sub>2</sub> and eliminated matrix cracking in SCS-6 reinforced composites even after thermal cycling. The SCS-6 fiber reinforcement improved the room temperature fracture toughness by seven times and impact resistance by five times. The composite exhibited excellent strength and toughness improvement up to 1400 °C. More recently, tape casting was adopted as the preferred processing of MoSi<sub>2</sub>-base composites for improved fiber spacing, ability to use small diameter fibers, and for lower cost. Good strength and toughness values were also obtained with fine diameter Hi-Nicalon tow fibers. This hybrid composite remains competitive with ceramic matrix composites as a replacement for Ni-base superalloys in aircraft engine applications.

## 1. INTRODUCTION

Advanced high temperature materials are key to successfully developing the next generation aerospace propulsion and power systems [1]. Advanced materials will enhance the performance of these systems by allowing higher speeds, expanded flight ranges, and increased payload capabilities. Due to high specific strength and stiffness, and the potential for increased temperature capability, composite materials are attractive for systems ranging from subsonic commercial aircraft to future space propulsion and power systems. Based on high temperature oxidation behavior, it appears that  $\text{MoSi}_2$  is one of the few intermetallics to have potential for further development. Since  $\text{MoSi}_2$  is a silica former, it can withstand at least 200 °C higher temperatures (up to 1500 °C) than alumina formers such as  $\text{NiAl}$  [2]. It also has a higher melting point (2023 °C) and lower density (6.2 g/cm<sup>3</sup>) than superalloys, and has electrical and thermal conductivity advantages over ceramics [3].

However, the use of  $\text{MoSi}_2$  has been hindered due to the brittle nature of the material at low temperatures, inadequate creep resistance at high temperatures, accelerated ('pest') oxidation at temperatures between approximately 450 and 550 °C, and its relatively high coefficient of thermal expansion (CTE) compared to potential reinforcing fibers such as  $\text{SiC}$ . The CTE mismatch between the fiber and the matrix results in severe matrix cracking during thermal cycling.

In the last twelve years, an extensive amount of work has been carried out in efforts to improve the high temperature properties of  $\text{MoSi}_2$  by solid solution alloying, discontinuous reinforcement, and fiber reinforcement. Alloying with W [4] or Re [5] has improved high temperature creep strength. Substantial improvements in strength have also been achieved by adding particulates, platelets or whiskers of  $\text{SiC}$  [6],  $\text{TiB}_2$ , and  $\text{HfB}_2$  [7]. However, the effects of grain refinement may limit the creep strength of these types of composites [8]. To date,  $\text{MoSi}_2$  alloyed with W and containing 40 vol %  $\text{SiC}$  has achieved the creep strength superior to that of the superalloys, although not the best monolithic ceramics. The addition of  $\text{SiC}$  whiskers has also yielded improvements in room temperature toughness [9]. However, it appears that the strength and damage tolerance required for high temperature aerospace applications can only be achieved by reinforcement with high strength continuous fibers.

Nb fibers [10] have been shown to improve the strength and toughness but this option is limited by a severe reaction between the Nb fiber and  $\text{MoSi}_2$ . Maloney and Hecht [11] have done extensive work on the development of continuous fiber reinforced  $\text{MoSi}_2$  base composites to achieve high temperature creep resistance and room temperature toughness. Candidate fibers consisted of such as  $\text{SiC}$ , single crystal  $\text{Al}_2\text{O}_3$ , ductile Mo, and W alloy fibers. The refractory metal fibers increased both creep strength and fracture toughness, although reaction with the matrix was still a problem. The addition of about 40 vol % of  $\text{SiC}$  in the form of whiskers and particulate was used to lower the thermal expansion of the  $\text{MoSi}_2$  base

matrix and prevented matrix cracking in these composites. However, matrix cracking was still observed in an SCS-6 fiber reinforced composite even with the matrix containing up to 40 vol % SiC whiskers. This composite also suffered catastrophic pest attack at 500 °C. Sapphire fiber reinforced composites showed no evidence of matrix cracking due to the good thermal expansion match between MoSi<sub>2</sub> and Al<sub>2</sub>O<sub>3</sub>. However, the strong fiber-matrix bond did not provide any toughness improvement.

MoSi<sub>2</sub> has been known to be susceptible to pesting, which is usually defined as disintegration into powder, and appears to be most pronounced near 500 °C [12-14]. The pesting phenomenon in MoSi<sub>2</sub> is considered to result from accelerated oxidation, which involves the simultaneous formation of MoO<sub>3</sub> and SiO<sub>2</sub> in amounts essentially determined by the Mo and Si concentrations in the intermetallic. The accelerated oxidation is a necessary but not sufficient condition for pesting. In some but not all cases, pesting has been linked to the formation of voluminous Mo oxides in porosity or microcracks. Improvements in fabrication of MoSi<sub>2</sub> have led to materials which had less porosity and were less susceptible to pest attack. Because of increased surface areas and complexities of fabrication from incorporating reinforcement phases in MoSi<sub>2</sub> based composites, pesting of composite materials is still a major concern [11,13]. Microalloying with Ge [15] and macroalloying with Cr [16] have also been shown to improve pesting resistance.

In earlier work [17] of developing MoSi<sub>2</sub> suitable for SiC fiber reinforcement, it was found that the addition of about 30 to 50 vol % of Si<sub>3</sub>N<sub>4</sub> particulate to MoSi<sub>2</sub> improved the low temperature accelerated oxidation resistance by forming a Si<sub>2</sub>ON<sub>2</sub> protective scale and thereby eliminated catastrophic pest failure. The Si<sub>3</sub>N<sub>4</sub> addition also improved the high temperature oxidation resistance and compressive strength. The brittle-to-ductile (BDTT) transition-temperature of MoSi<sub>2</sub>-30vol%Si<sub>3</sub>N<sub>4</sub>, measured in 4 point bending, was between 900 and 1000 °C. More importantly, the Si<sub>3</sub>N<sub>4</sub> addition significantly lowered the CTE of the MoSi<sub>2</sub> and eliminated matrix cracking in SCS-6 reinforced composites even after thermal cycling [14,18].

These encouraging preliminary results led to a joint program for further development between Pratt & Whitney, the Office of Naval Research, and NASA Lewis. The overall technical direction of this long range program is to develop this composite system for advanced aircraft engine application as a competitor to both today's superalloys and other advanced materials, primarily ceramic matrix composites. A turbine blade outer air seal for Pratt and Whitney's ATEGG/JTD engine demonstrator was chosen as the first component upon which to focus. This paper briefly describes the progress made so far in developing, processing, and characterizing MoSi<sub>2</sub> base hybrid composites.

## **2. MATERIALS AND PROCEDURES**

Attrition milling of  $\text{MoSi}_2$  and  $\text{Si}_3\text{N}_4$  powder is the first step in composite processing. Several batches containing a mixture of commercially available  $\text{MoSi}_2$  and either 30 or 50 vol % of  $\text{Si}_3\text{N}_4$  were mechanically alloyed in a Union Process attritor. No densification aids were added to the  $\text{MoSi}_2$ - $\text{Si}_3\text{N}_4$  mixtures. The average mean particle size of the mixture after milling was  $1.25 \pm 0.71 \mu\text{m}$  at 99 percent confidence. The  $\text{MoSi}_2$ - $\text{Si}_3\text{N}_4$  powder was consolidated into “matrix-only” plates 12 cm long  $\times$  5 cm wide  $\times$  0.3 cm thick, or a larger size of 18 cm long  $\times$  2.5 cm wide  $\times$  1.25 cm thick. The plates were consolidated by vacuum hot pressing followed by hot isostatic pressing (HIP) to achieve full density. Composite plates of various thickness consisting of 6, 12, or 56 plies of 30 vol % SCS-6 fibers having 0, 0/90 and 90 orientations in a  $\text{MoSi}_2$ - $\text{Si}_3\text{N}_4$  matrix were prepared by the powder cloth technique [15] and consolidated in the same manner as the material without fibers. The two-step consolidation process enabled the use of a lower consolidation temperature than could be used if hot pressing was used alone. This resulted in fully dense material without excessive reaction or damage to the fibers.

From the consolidated material, ASTM standard specimens for several tests such as compression, fracture toughness, impact and oxidation were machined by electrodischarge machining (EDM) and grinding techniques. Tensile tests were conducted on  $1.27 \times 15$  cm straight or dog bone-shaped specimens machined from 6 ply composite panels. Tests were performed in air between 25 and 1200 °C at constant strain rate of  $1.4 \times 10^{-3}$ . Constant load compression creep tests were conducted on  $\text{MoSi}_2$ -50 $\text{Si}_3\text{N}_4$  cylindrical specimens (5 mm diameter  $\times$  10 mm long) at 1200 °C in the stress range of 40 to 500 MPa in air. Fracture toughness tests were measured on chevron notched bend specimens made from 12 ply composite panels, tested at a constant strain rate of  $1.2 \times 10^{-5}$  cm/min. Constant stress-rate tests were carried out to assess the slow crack behavior of  $\text{MoSi}_2$ -50 $\text{Si}_3\text{N}_4$  having two batches with two different densities in flexure at 1200 °C in air using standard 3 mm wide  $\times$  4 mm thick  $\times$  25 mm long specimens. ASTM full size (12 mm<sup>2</sup> cross section  $\times$  52 mm long) Charpy V-notch impact specimens were machined from both  $\text{MoSi}_2$ -50 $\text{Si}_3\text{N}_4$  monolithic and 56 ply hybrid composites and impact tests were conducted using 356 J Tinus Olsen impact tester with Dynatrup instrumentation. The heating of the specimen was carried out using two oxypropane torches. The temperature was monitored using a laser pyrometer. Tensile creep-rupture tests were performed in vacuum between 1100 to 1200 °C at 70 MPa were conducted on hybrid composites using an MTS machine fitted with water cooled grips and a side-contact extensometer. Cyclic oxidation coupons typically were  $1.2 \times 1.2 \times 0.25$  cm and were ground and polished to final 1  $\mu\text{m}$  diamond polish. In the case of composites, no attempt was made to coat the exposed fibers.

Detailed microstructural characterization of as-fabricated and tested specimens were carried out using standard optical and electron microscopic techniques.

### **3. RESULTS AND DISCUSSION**

#### ***3.1: Microstructure of As-fabricated Materials***

Figure 1 (a) shows the microstructure of the as-consolidated  $\text{MoSi}_2\text{-Si}_3\text{N}_4$  monolithic matrix. The  $\text{Si}_3\text{N}_4$  particles are interconnected and well dispersed in the  $\text{MoSi}_2$  matrix. As the volume fraction of  $\text{Si}_3\text{N}_4$  particulate increased, the degree of interconnectivity of the  $\text{Si}_3\text{N}_4$  phase increased, although even at 50 vol % nitride, the materials could still be machined by EDM. As expected from thermodynamic predictions, the  $\text{Si}_3\text{N}_4$  particles appeared to be quite stable, with very little or no reaction with the  $\text{MoSi}_2$  even after exposure at 1500 °C. X-ray diffraction of  $\text{MoSi}_2\text{-Si}_3\text{N}_4$  showed only the presence of  $\text{MoSi}_2$  (tetragonal) and a mixture of alpha and beta  $\text{Si}_3\text{N}_4$  phases. Even though there is a significant CTE mismatch between  $\text{MoSi}_2$  and  $\text{Si}_3\text{N}_4$ , the small particle size prevented thermally induced microcracking. TEM examination, Fig. 1(b), performed on  $\text{MoSi}_2\text{-Si}_3\text{N}_4$  also confirmed no reaction between  $\text{MoSi}_2$  and  $\text{Si}_3\text{N}_4$ . In some isolated areas very fine  $\text{Mo}_5\text{Si}_3$  phase was detected. This is believed to have been present in the as-procured  $\text{MoSi}_2$  powder. Figure 2 shows the transverse microstructure of the as-fabricated SCS-6/ $\text{MoSi}_2\text{-Si}_3\text{N}_4$  composite. A reaction zone around the fibers was generally <1  $\mu\text{m}$  in thickness and resulted from reaction of the carbon layer to form  $\text{SiC}$  and  $\text{Mo}_5\text{Si}_3$ . Although the fiber distribution is not uniform, Fig. 2 indicates the absence of matrix cracking. The CTE measurements made on the matrix-only plate and composites plotted as a function of temperature are compared with the monolithic constituents in Fig. 3. It is clear from Fig. 3 that the addition of  $\text{Si}_3\text{N}_4$  to  $\text{MoSi}_2$  has effectively lowered the CTE of the matrix, achieving the desired result of eliminating matrix cracking. Furthermore, no cracks were found in either the matrix or the reaction zone even after 1000 thermal cycles between 1200 and 200 °C in vacuum. These results show that the use of  $\text{Si}_3\text{N}_4$  was much more effective than similar attempts [9] using  $\text{SiC}$ .

#### ***3.2: Oxidation Behavior of $\text{MoSi}_2$ -Base Composites:***

##### ***3.2.1: Low temperature oxidation***

Since the low temperature oxidation and pesting phenomenon are limiting factors for structural applications of  $\text{MoSi}_2$ -base composites, several critical tests were designed to examine the pesting response. Initially, cyclic oxidation tests were conducted at 400, 500 and 600 °C for 200 cycles. Each cycle consisted of 55 min of heating and 5 min of cooling. The weight gain at 500 °C was comparatively higher than at 400 and 600 °C, which again confirms the previous observation [10] that 500 °C is the temperature

for maximum accelerated oxidation/pest for  $\text{MoSi}_2$ -base alloys. It was therefore decided that 500 °C would be used for all subsequent experiments to examine the oxidation behavior in more detail.

Figure 4(a) shows the specific weight gain versus number of cycles at 500 °C. Both  $\text{MoSi}_2$ -30 $\text{Si}_3\text{N}_4$  and 50  $\text{Si}_3\text{N}_4$  show very little weight gain indicating the absence of accelerated oxidation. X-ray diffraction analysis of both these specimens indicated strong peaks of  $\text{Si}_2\text{ON}_2$  and the absence of  $\text{MoO}_3$ . The  $\text{MoSi}_2$  exhibited accelerated oxidation followed by pesting. Initial TEM studies on 500 °C/50 cycles oxidized  $\text{MoSi}_2$  samples indicated that oxide formed on  $\text{MoSi}_2$  is a two phase lamellar structure as shown in Fig. 4(b) consisting of  $\text{MoO}_3$  and amorphous  $\text{SiO}_2$ . This kind of lamellar structure could provide an easy diffusion path for oxygen, favoring the formation of the  $\text{MoO}_3$ . The TEM examination of a  $\text{MoSi}_2$ -30  $\text{Si}_3\text{N}_4$  specimens oxidized at 500 °C for 1000 hr, Fig. 4(c), showed an order of magnitude decrease in oxide thickness and a disruption of the lamellar oxide structure. However, fine features of the scale in Fig. 4(c) have not been analyzed.

Several critical oxidation tests were carried out at 500 °C to examine the influence of pre-existing cracks and superimposed stresses on  $\text{MoSi}_2$ -30  $\text{Si}_3\text{N}_4$  materials. These tests included oxidation of bend bars which were precracked using 250 N load and a Vickers indenter. Both uncracked and precracked specimens were oxidized under unstressed, compressive, or tensile stresses. All these tests were extended to 1000 hr, with no indications of pesting or premature failure. Finally, burner rig tests were conducted using a jet fuel on two specimens with different degrees of surface roughness, and both specimens came out without showing any evidence of pesting.

Under similar conditions the hybrid composite specimens showed much less weight gain than the matrix-only material. However, the carbon layer on the exposed ends of SCS-6 fibers did oxidize, which influenced the weight gain measurement. Figure 5 shows the SCS-6/ $\text{MoSi}_2$  and SCS-6/ $\text{MoSi}_2$ -30 $\text{Si}_3\text{N}_4$  composites exposed at 500 °C. The SCS-6/ $\text{MoSi}_2$  specimen, which had matrix cracks, was completely disintegrated into powder within 24 cycles, whereas the SCS-6/ $\text{MoSi}_2$ -30 $\text{Si}_3\text{N}_4$  specimen was intact even after 200 cycles. This is again in strong contrast to previous work [11], where both SCS-6/ $\text{MoSi}_2$ -40 vol % SiC and  $\text{Al}_2\text{O}_3$ / $\text{MoSi}_2$  composites were reduced to powder after exposure at 500 °C. All of these observations are consistent with the elimination of pest attack in  $\text{MoSi}_2$ - $\text{Si}_3\text{N}_4$  composites due to a mechanism involving elimination of the accelerated oxidation associated with a non-protective  $\text{MoO}_3$  oxide scale. The  $\text{Si}_2\text{ON}_2$  scale forms rapidly, and is protective even at cracks, pores, and interfaces.

### 3.2.2 High temperature oxidation behavior:

The results of cyclic oxidation tests at 1250 °C, which more closely approximates the conditions under which the material would be subjected in a structural application, are shown in Fig. 6. The materials in Fig. 6 were subjected to one hour heating cycles to 1250 °C, followed by twenty minute cooling cycles. It



can be seen that the  $\text{MoSi}_2$ -50  $\text{Si}_3\text{N}_4$  particulate composite exhibited superior oxidation resistance as compared to  $\text{MoSi}_2$  alone. The specific weight gain of  $\text{MoSi}_2$ -50 $\text{Si}_3\text{N}_4$  was only about 1 mg/cm<sup>2</sup> in 1000 hr, almost comparable to CVD SiC, which is considered the best  $\text{SiO}_2$  former available. The composite initially lost weight due to oxidation of the carbon on the SCS-6 fiber. This was followed by steady weight gain, less than 2 mg/cm<sup>2</sup> in 1000 hr. X-ray diffraction of surface oxides on  $\text{MoSi}_2$ -50  $\text{Si}_3\text{N}_4$  and hybrid composites indicated strong peaks of  $\alpha$ -cristobalite, which is a crystalline form of  $\text{SiO}_2$  and a protective oxide.

### **3.3. Mechanical Properties of $\text{MoSi}_2$ - $\text{Si}_3\text{N}_4$ :**

#### **3.3.1 Compressive creep behavior**

Previous work [17,18] showed that the nitride additions substantially increased compressive strength at all temperatures. This has been augmented with additional testing to further characterize this material. Figure 7 shows the results of constant load compression creep tests at 1200 °C on  $\text{MoSi}_2$ -50 $\text{Si}_3\text{N}_4$  plotted as second stage creep rate ( $\dot{\epsilon}$ ) versus specific stress. For comparison, several materials such as  $\text{MoSi}_2$ ,  $\text{MoSi}_2$ -40SiC [8], and a single crystal Ni- base superalloy [20] are also included.  $\text{MoSi}_2$ -50 $\text{Si}_3\text{N}_4$  is almost five orders of magnitude stronger than binary  $\text{MoSi}_2$  and comparable to  $\text{MoSi}_2$ -40SiC. This again confirms the previous observation of beneficial effects of particulate reinforcement. The derived stress exponent,  $n = 5.3$ , and the activation energy = 520 kJ/mol calculated from the temperature dependence of creep rate at constant stress, [6] imply a diffusion controlled dislocation mechanism as the rate controlling mechanism.

#### **3.3.2 Fracture toughness behavior**

The fracture toughness of  $\text{MoSi}_2$  and  $\text{MoSi}_2$ - $\text{Si}_3\text{N}_4$  base materials were measured on chevron notched 4 point bend specimens. A finite element/slice model was used to calculate  $K_{\text{Ic}}$  [21]. Figure 8(a) shows the plot of fracture toughness of  $\text{MoSi}_2$ -50 $\text{Si}_3\text{N}_4$  as a function of temperature. For comparison, two monolithic ceramics SiC and  $\text{Si}_3\text{N}_4$  are also included in the figure [22]. The room temperature fracture toughness of both  $\text{MoSi}_2$ -30 $\text{Si}_3\text{N}_4$  and 50 $\text{Si}_3\text{N}_4$  matrix was ~5.2 MPa√m, which is about twice the value measured on monolithic  $\text{MoSi}_2$ . Further improvement in room temperature fracture toughness of  $\text{MoSi}_2$ - $\text{Si}_3\text{N}_4$  can be achieved by (a) microalloying  $\text{MoSi}_2$  with elements like Nb, Al, and Mg (b) by growing randomly oriented long whisker type  $\beta$ - $\text{Si}_3\text{N}_4$  grains. Preliminary results of fracture toughness tests on  $\text{MoSi}_2$ - $\text{Si}_3\text{N}_4$  base materials developed by these two approaches are very encouraging. As an example, Fig. 8(b) shows the microstructure of  $\text{MoSi}_2$ -50 $\text{Si}_3\text{N}_4$  where the  $\alpha$ - $\text{Si}_3\text{N}_4$  grains were grown in the form of randomly oriented whisker type  $\beta$ - $\text{Si}_3\text{N}_4$  by proper choice of consolidation and heat treatment. The room temperature fracture toughness test results shown in Fig. 8(c) indicates that almost three times

improvement in fracture toughness in MoSi<sub>2</sub>-50βSi<sub>3</sub>N<sub>4</sub> material compared to the conventional MoSi<sub>2</sub>-Si<sub>3</sub>N<sub>4</sub> material. Figure 8(a) also shows that fracture toughness of MoSi<sub>2</sub>-Si<sub>3</sub>N<sub>4</sub> increases with temperature, especially beyond 1000 °C, which is the BDTT for this material. The ceramics chosen for comparison were made by hot pressing techniques that are similar to those used to make MoSi<sub>2</sub>. *In situ* toughened Si<sub>3</sub>N<sub>4</sub> [23] exhibits higher toughness values, approaching 10 MPa√m. But, all of the ceramics maintain the same toughness as temperature is increased.

### 3.3.3 Slow crack growth behavior

Constant stress-rate (also called "dynamic fatigue") testing for the test specimens was conducted in flexure at 1200 °C in air to evaluate slow crack growth (SCG). Three different loading rates ranging from 40 to 40,000 N/min, with corresponding stress rates from 0.33 to 333 MPa/s, were applied to the test specimens by the testing machine under load-control. The use of lower stress rate was avoided to minimize a possible creep deformation, thus to obtain slow crack growth as a unique mechanism associated with failure. Details of experimental procedures and calculations are described elsewhere [24-26]. A total of four specimens were used at each stress rate. Each specimen was kept at the test temperature for about 20 min prior to testing.

TABLE 1.—BASIC PHYSICAL AND MECHANICAL PROPERTIES OF MoSi<sub>2</sub>-50 vol % Si<sub>3</sub>N<sub>4</sub> COMPOSITES

Material	Density, <sup>a</sup> g/cm <sup>3</sup>	Young's modulus, <sup>b</sup> GPa	Hardness, <sup>c</sup> GPa	Fracture toughness, <sup>d</sup> MPa√m
Batch 1	4.33±0.04 (4) <sup>e</sup>	315±10 (4)	16.2±2.6 (5)	4.94±0.32 (4)
Batch 2	4.20±0.01 (5)	248±16 (5)	11.4±1.1 (4)	3.52±0.44 (3)

<sup>a</sup>By mass/volume method.

<sup>b</sup>By impulse excitation method (ASTM C1259).

<sup>c</sup>By Vickers hardness indentation method (ASTM C 1327).

<sup>d</sup>By the single edge precracked beam (SEPB) method (ASTM PS070).

<sup>e</sup>The parenthesis indicates the number of specimens used.

The results of constant stress-rate testing for the two batches tested at 1200 °C in air are shown in Fig. 9(a). A decrease in strength with decreasing stress rate, which represents the susceptibility to slow crack growth, is evident for the two materials. The slow crack growth for Batch 1 was moderate with a value of  $n = 34.8$  while the SCG for the second batch was significant with  $n = 14.6$ . In other words, the first batch exhibited higher SCG resistance than the second batch. Also note that overall strengths were greater in the first batch than in the second batch. A slight increase in porosity exhibited by the second

batch resulted in both appreciable susceptibility to SCG and lower strength. Hence, a careful control in density is extremely important for this  $\text{MoSi}_2\text{-Si}_3\text{N}_4$  composite system.

A convenient way to see the effect of slow crack growth on lifetime is to construct a lifetime prediction diagram, based on the lifetime-versus-applied stress relation ("static fatigue" diagram). This can be done by using the following relation

$$t_{fs} = \frac{1}{(n+1)} t_{fd} \quad (1)$$

where  $t_{fs}$  is the lifetime converted and  $t_{fd}$  is the time to failure determined in the constant stress-rate testing. The resulting lifetime diagram is depicted in Fig. 9(b). The data of NC132 silicon nitride [27] were included for comparison purpose. It was assumed that slow crack growth is a major mechanism associated with failure at this temperature (1200 °C). This figure clearly illustrates a great difference in SCG behavior between the two composite materials: the lifetime for a given level of applied stress is much greater in the first batch than in the second batch. Also, between the first batch and NC132 silicon nitride, the lifetime reliability at the lower levels of applied stresses (probably close to the actual service condition) is better for the first batch than NC 132 silicon nitride. Hence, in terms of long-term reliability, the first batch is the most desirable material among the three materials.

### **3.4 Mechanical Properties of SCS-6/ $\text{MoSi}_2\text{-Si}_3\text{N}_4$ Hybrid Composites:**

#### **3.4.1 Fracture toughness behavior:**

Figure 10 shows the load verses displacement plot for SCS-6/ $\text{MoSi}_2\text{-30Si}_3\text{N}_4$  monolithic chevron notched 4 point bend specimens tested at room temperature. The composite specimen did not break even after testing for 2 hr. The apparent critical stress intensity factor,  $K_{Ic}$ , calculated from the maximum load data was greater than 35  $\text{MPa}\sqrt{\text{m}}$ , which is 7 times tougher than the monolithic material. The toughness of the hybrid composite also increased with temperature reaching as high as 65  $\text{MPa}\sqrt{\text{m}}$ , at 1400 °C in argon atmosphere.

#### **3.4.2 Tensile Behavior**

Figure 11(a) shows the room temperature tensile nominal stress strain curve for SCS-6/ $\text{MoSi}_2\text{-Si}_3\text{N}_4$ , indicating composite-like behavior; and three distinct regions, an initial linear region, followed by a nonlinear region and a second linear region. The nonlinear region is due to the matrix cracking normal to the loading direction. The second linear region is controlled by fiber bundle strength. Individual SCS-6 fibers were tensile tested at room temperature in the as-received, as-etched and etched-from-composite

conditions, and produced average strength values of  $3.52 \pm 0.8$ ,  $3.35 \pm 0.6$ , and  $3.4 \pm 1$  GPa, respectively. Thus, neither etching nor consolidation conditions degraded the strength of the fibers, and SEM examination of the fiber surfaces showed no visible differences among the three fiber conditions.

Fiber/matrix interfacial properties play an important role in composite mechanical behavior. In the case of this composite system, the carbon layer on SCS-6 provides an appropriate level of bonding that produces adequate strengthening and toughening. The carbon can react with  $\text{MoSi}_2$  to form  $\text{SiC}$  and  $\text{Mo}_5\text{Si}_3$ , although the carbon layer is still retained and the reaction zone thickness is not very large at typical HIP temperatures. The fiber matrix interfacial shear strengths determined from a fiber push out test [28] using thin polished sections produced values near 50 MPa, indicating a weak bond between the matrix and the fiber. In comparison the interfacial shear strength for SCS-6/reaction bonded silicon nitride (RBSN) is about 30 MPa [28].

It was found that the room temperature ultimate tensile strength and strain to fracture were reduced by only 20 percent in a specimen with exposed fibers preoxidized at 1200 °C for 200 hr. Alternatively, a different, higher strength lot of fibers could be responsible for this result. High temperature tensile tests were performed in air at temperatures up to 1400 °C. This is believed to be an advantage over CMC's which exhibit matrix cracking at all temperatures. Figure 11(b) shows the temperature dependence of ultimate tensile strength, along with the data from competitive materials, namely single crystal PWA1480 [29], and SCS-6/reaction bonded silicon nitride (RBSN) [30]. PWA 1480 exhibits higher tensile strength than both  $\text{MoSi}_2$ -base and RBSN-base composites between room temperature and 1000 °C; however, PWA 1480 is almost 3 times denser than both composites, and hence is at a disadvantage on a specific strength basis. Although not included in Fig. 11(b) because of different fiber and architecture, typical two-dimensional woven  $\text{SiC-SiC}$  composites [31] exhibit much lower strengths ( $\sim 200$  MPa) between room temperature and 1200 °C. However,  $\text{SiC-SiC}$  composites retain their strengths beyond 1200 °C. Figure 11(b) also shows the tensile strength data for the SCS-6 fibers, re-emphasizing the fiber-dominated behavior of the composites. The  $\text{MoSi}_2$ -base composites also exhibited elastic modulus values of  $\sim 290/200$  GPa between RT and 1200 °C which were substantially higher than the comparable CMC at all temperatures. Unlike most CMC's which have as much as 20 percent porosity, these  $\text{MoSi}_2$ -base composites are fully dense and hence exhibit higher modulus.

Several tensile creep tests were carried out on SCS-6<sub>[0]</sub>/ $\text{MoSi}_2$ -50 $\text{Si}_3\text{N}_4$  composite specimens between 1000 and 1200 °C in vacuum. Unfortunately, it was not possible to get the rupture lives from these tests due to accidental power failures. Nonetheless, test durations of  $\sim 1000$  hr were achieved and some idea of long term durability was obtained. Specimens tested at these temperatures exhibited a short primary creep stage and an extended secondary stage. The minimum creep rates ranged from  $1.0 \times 10^{-9}$  to  $2.0 \times 10^{-9}$  s<sup>-1</sup> at 70 MPa between 1100 and 1200 °C.

### 3.4.3 Impact Behavior:

Aircraft engine components require sufficient toughness to resist manufacturing defects, assembly damage, stress concentrations at notches, and foreign and domestic object damage [32]. Consultation with engine company designers indicated a strong desire for not only fracture toughness but more importantly, impact resistance to be measured before they would seriously consider these types of composites. The Charpy V-notch (CVN) test was chosen to assess impact resistance based on the engine designer's desire to use a relative ranking against more familiar materials, rather than a formal design requirement.

CVN impact tests were conducted on full size specimens of  $\text{MoSi}_2$ - $50\text{Si}_3\text{N}_4$  matrix and SCS-6<sub>[0]</sub> and <sub>[0/90]</sub> oriented / $\text{MoSi}_2$ - $50\text{Si}_3\text{N}_4$  hybrid composites between liquid nitrogen temperature (-300 °C) and 1400 °C in air. Figure 12(a) shows the force time curves obtained from the instrumented impact tests at room temperature for monolithic  $\text{MoSi}_2$ - $50\text{Si}_3\text{N}_4$ , SCS-6<sub>[0]</sub> and <sub>[0/90]</sub>/ $\text{MoSi}_2$ - $50\text{Si}_3\text{N}_4$  composites. The maximum value of force represents the elastic energy required for crack initiation. The hybrid composite in [0] orientation exhibited the highest peak force values, followed by the cross-ply and finally the monolithic material. At 1400 °C, the peak force values for all three materials were higher than their corresponding values at room temperature. The hybrid composite exhibited a gradual, stepwise decrease in load after the peak force was achieved. This indicates substantial energy absorption during crack propagation, and was especially pronounced in the [0] orientation.

Figure 12 (b) shows the temperature dependence of CVN energy for  $\text{MoSi}_2$ -base materials compared with other potential materials such as superalloys, and ceramics. The CVN energy for both the monolithic  $\text{MoSi}_2$ - $50\text{Si}_3\text{N}_4$  and the hybrid composites increased with increasing temperature. The fiber reinforcement in [0] orientation increased the impact resistance by 5 times and in [0/90] orientation nearly two times. The CVN energy of SCS-6/ $\text{MoSi}_2$ - $50\text{Si}_3\text{N}_4$  was comparable to the cast superalloy B-1900 but substantially lower than the wrought superalloy Hastelloy X. The CVN energy of  $\text{MoSi}_2$ - $50\text{Si}_3\text{N}_4$  monolithic was comparable to Mo alloys and in-situ toughened  $\text{Si}_3\text{N}_4$  (AS-800) and was far superior to NiAl [34], and monolithic hot pressed  $\text{Si}_3\text{N}_4$ , and SiC. Unlike  $\text{MoSi}_2$ - $50\text{Si}_3\text{N}_4$  which shows increased CVN energy with temperature (beyond 1000 °C), the AS-800 shows a constant CVN energy between -300 and 1400 °C. The monolithic SiC shows a slight decrease of CVN energy with temperature. This is probably due to the degradation caused by densification aids used with SiC [33]. SEM examination of impact tested SCS-6/  $\text{MoSi}_2$ -50  $\text{Si}_3\text{N}_4$  showed substantial fiber pullout in [0] orientation and limited fiber pullout in [0/90] oriented specimens at all temperatures. Additionally, the SEM image Fig. 13(a) showed substantial matrix cracking in the room temperature tested specimens, but only limited cracking at 1400 °C Fig. 13(b). This again implies that  $\text{MoSi}_2$  can behave in a ductile manner at higher temperatures.

### ***3.5 Technological Needs: Complex Shapes and Low Cost Processing:***

Most of the attractive strength and toughness values reported so far were achieved with composites reinforced with SCS-6 fibers made by Textron, Inc. This large diameter (145  $\mu\text{m}$ ) fiber was designed primarily for Ti-based composites. This fiber does not have adequate creep strength at the highest temperatures envisioned for  $\text{MoSi}_2$  and is too large to be bent around the sharp radii needed to make complex shapes. However, it is easy to infiltrate matrix powders between these fibers, thus enabling composites to be fabricated routinely. This ease in fabrication was meant to be exploited by further characterization of key properties such as creep resistance, transverse properties, and performance of the composite in an engine test bed. However, finer diameter fibers are preferred on a cost, shape making, creep resistance, and toughness basis. Hi-Nicalon is the best currently available fiber, although Dow Corning's Sylramic® fiber, developed for the NASA High Speed Civil Transport program, is also appropriate for this  $\text{MoSi}_2$ - $\text{Si}_3\text{N}_4$  matrix. A transition in effort to Hi-Nicalon fibers was therefore investigated, first using tow fibers, (i.e., strings of approximately 500 individual filaments that are spread out, wound on a drum and then infiltrated with matrix powder) and ultimately woven cloth (i.e., the tows are woven into two or three dimensional architectures before matrix infiltration).

In earlier studies, the powder cloth technique was used to produce SiC continuous fiber reinforced  $\text{MoSi}_2$ -base composites. The powder cloth process is labor intensive and cannot always produce a uniform fiber distribution. Melt infiltration and chemical vapor infiltration are popular methods for processing of CMC's because of the potential for shape making and lower cost, but are limited to thickness on the order of 5 mm, because segregation and porosity problems are aggravated in thick specimens. Tape casting was therefore adopted as a powder metallurgy method for composite fabrication. Initially, several casting trials of  $\text{MoSi}_2$ - $\text{Si}_3\text{N}_4$  were carried out to optimize various parameters such as particle size, type and amount of binder and solvent, flow behavior of the slurry, and binder burn-out cycle. A 56 ply composite of SCS-6/ $\text{MoSi}_2$ - $\text{Si}_3\text{N}_4$  was successfully fabricated by tape casting followed by the standard hot press plus HIP consolidation. Composites with small diameter fibers such as SCS-9 (75  $\mu\text{m}$ ) and coated Hi-Nicalon (18 to 20  $\mu\text{m}$ ) were also successfully fabricated. Figure 14 illustrates the range in fiber diameters in this study. Note also the improvement in fiber spacing control between Figs. 14(a) and (b) achieved by switching from powder cloth to tape casting. Figure 15 displays efficient spreading of the fiber tows and infiltration of  $\text{MoSi}_2$ - $\text{Si}_3\text{N}_4$  powder particles. Although there is still some heterogeneity in the fiber distribution, this microstructure is among the best we have seen on any other study using fine diameter fibers.

Interfacial coatings play a very important role in fiber reinforced composites, and the Hi-Nicalon tow fibers must be coated before reinforcing the  $\text{MoSi}_2$ - $\text{Si}_3\text{N}_4$  matrix. Interfacial coatings that have proven successful in CMC's have been adopted for use with  $\text{MoSi}_2$ . To date, only carbon or BN have been able to

provide the level of interfacial bonding required for toughening, but they both exhibit poor environmental resistance. Therefore, a protective coating of SiC or Si<sub>3</sub>N<sub>4</sub> is required as a second layer on top of the debonding layer. Unfortunately, the state of coating technology for fine diameter tows has still not matured to the state where smooth, crack free and uniformly thick coatings can be produced. This immaturity is also reflected in the high cost and limited facilities nationally available for coating. Therefore, only limited mechanical properties have been generated with these fibers.

### **3.6. Influence of fiber diameter and architecture on Mechanical properties**

The influence of fiber diameter and architecture on mechanical properties was investigated by conducting room temperature tensile and fracture toughness tests on specimens of SCS-6, SCS-9 and BN/SiC coated Hi-Nicalon/MoSi<sub>2</sub>-50Si<sub>3</sub>N<sub>4</sub> hybrid composites. Testing in the [0] direction (longitudinal) produced the highest strength, (700 to 1000 MPa strength and 1.2 percent total strain) to failure. Testing in the [90] direction produced the lowest ultimate tensile strength of only 72 MPa and 0.04 percent strain to failure for SCS-6 reinforced composite. This is not an unexpected result since the fibers cannot bridge matrix cracks in the transverse direction, and cross-plyed laminates or woven two- or three-dimensional architectures are required to achieve more isotropic properties. For example, the Hi-Nicalon reinforced composite exhibited high strength and strain to failure in the 0/90 architecture, about 60 percent of the unidirectional value, Fig. 16(a). Figure 16(b) shows that the Hi-Nicalon/MoSi<sub>2</sub>-Si<sub>3</sub>N<sub>4</sub> in [0/90] direction exhibited higher fracture toughness than the CMC's Hi-Nicalon/SiC and Hi-Nicalon/Si<sub>3</sub>N<sub>4</sub>, even though they were tested in the more favorable [0] direction [35]. The CMC's were processed at much higher temperatures, 1600 to 1800 °C, causing more fiber degradation than Hi-Nicalon/MoSi<sub>2</sub>-Si<sub>3</sub>N<sub>4</sub> and therefore exhibited lower toughness. The SEM micrograph of the fracture toughness tested Hi-Nicalon reinforced composite Fig. 17(a) showed more fiber pullout than the SCS-6 fiber reinforced composite Fig. 17(b).

Figure 18 shows the influence of fiber diameter and architecture on flexural stress rupture at 1200 °C/ 210 MPa in air. This figure clearly indicates the limited improvement with large diameter fiber and more than two orders of improvement with fine diameter fiber [0/90 oriented] in stress rupture lives. The SEM micrograph of stress ruptured Hi-Nicalon<sub>[0/90]</sub>/MoSi<sub>2</sub>-Si<sub>3</sub>N<sub>4</sub> composite showed substantial fiber pull out on the tension side of the specimen.

In order to respond to the industrial need of low cost processing of complex shaped MoSi<sub>2</sub>-base composites, it was decided to initiate the melt infiltration processing of two-dimensional woven Hi-Nicalon preforms. This kind of processing is being used for SiC/SiC composites. The preforms measuring 10 cm wide × 15 cm long × 0.3 cm thick and having a dual layer coating of BN and SiC by

chemical vapor infiltration were obtained from Dupont. The preforms were cut into several strips of 1.2 cm wide  $\times$  15 cm long. These strips were placed in a Plaster of Paris mold. A water based slurry of  $\text{MoSi}_2\text{-Si}_3\text{N}_4$  mixture having controlled pH was prepared. The slurry was vacuum infiltrated into the strips. About 50 vol % infiltration was achieved using this technique. The Slurry infiltrated pre-forms were dried and then infiltrated with molten silicon alloy to achieve full density. Preliminary results on microstructure and mechanical property of the melt infiltrated composites are promising. Work is in progress to optimize the slurry and melt infiltration processing parameters.

### ***3.7 Engine Testing of Hi-Nicalon/ $\text{MoSi}_2\text{-Si}_3\text{N}_4$ Hybrid Composite:***

Encouraged by the preliminary results on mechanical behavior of the hybrid composite, it was decided test this material in the aggressive environment of gas turbine engine. Two panels of the  $\text{BN/Si}_3\text{N}_4$  coated Hi-Nicalon<sub>(0.990)</sub>/ $\text{MoSi}_2\text{-50Si}_3\text{N}_4$  hybrid composite, approximately 12 cm long  $\times$  6 cm wide  $\times$  0.6 cm thick were fabricated by tape casting and hot pressing techniques. From the consolidated panels, two engine test coupons were made according to Pratt and Whitney's two versions of design. After machining, the surfaces of these coupons were coated with 2  $\mu\text{m}$  thick SiC by chemical vapor deposition (CVD) to protect the exposed fibers from environmental degradation. Only one test coupon was tested in Pratt and Whitney's demonstrator engine, XTC/66/b, to simulate the blade outer air seal (BOAS) thermal cyclic conditions. The test coupon with all instrumentation was placed about two inches behind the high pressure turbine blades in the engine. A small amount of clamping was used to hold the test coupon in place. One surface of the test coupon was facing the jet fueled flame, which reached approximately 1205 °C and produced a thermal gradient of about 600 °C between the exposed (front) and unexposed (back) surfaces. According to Eng (36) this hybrid composite performed significantly better than a SiC whisker reinforced  $\text{MoSi}_2$ , which showed several cracking within the first few cycles. The composite was removed after 15 cycles and post-test examination did not reveal any surface or matrix cracking.

## **4. CONCLUSIONS**

A wide spectrum of mechanical and environmental properties have been measured in order to establish feasibility of an  $\text{MoSi}_2$  base composite with  $\text{Si}_3\text{N}_4$  particulate and SiC fibers. The high impact resistance of the composite is of particular note, as it was a key property of interest for engine applications. Processing issues have also been addressed in order to lower cost and improve shape making capability. These results indicate that this composite system remains competitive with other ceramics as a potential replacement for superalloys.



## **Acknowledgments**

The author would like to acknowledge financial support from the Office of the Naval Research, (A.K. Vasudevan ), NASA-LeRC (M.V. Nathal), and Pratt & Whitney Aircraft, West Palm Beach, FL (W. Pospisil).

## **REFERENCES**

1. J.R. Stephens, Aviation Week and Space Technology, August 1992
2. J. Doychak, Journal of Metals, June (1992), pp. 46–51.
3. A.K. Vasudevan and J.J. Petrovic, High Temperature Silicides, Ed.by A.K. Vasudevan and J.J. Petrovic., North Holland, NY, 1992, pp. 1–17.
4. J.J. Petrovic and R.E. Honnell, Cerm. Eng. Soc. Proc., 11 (1990), pp. 734–744.
5. D.M. Shah and D.L. Anton, U.S. Airport Report WRDC-TR-90-4122, Feb. 1991.
6. S. Bose, High Temperature Silicides, Ed., A.K. Vasudevan and J.J. Petrovic. North-Holland, NY, 1992, pp. 217–225.
7. R.M. Aikin, Jr., Structural Intermetallics, Eds. R. Darolia, J.J. Lewandowski, C.T. Liu, D.B. Miracle, and M.V. Nathal, TMS, Warrendale, PA, 1993, pp. 791–798.
8. K. Sadananda, C.R. Feng and H. Jones., High Temperature Silicides. Ed., A.K. Vasudevan and J.J. Petrovic. North -Holland, NY, 1992, pp. 227–237.
9. J.J. Petrovic, R.E. Honnell and W.S. Gibbs, "Moly disilicide alloy matrix composites," US Patent, 4970,179.
10. E. Fitzner and W. Remmele, 5th Int. Conf. on Composite Materials, ICCM-V, AIME (1985), pp. 515–530.
11. M.J. Maloney and R.J. Hecht, High Temperature Silicides, Ed., A.K. Vasudevan and J.J. Petrovic, North Holland, NY, 1992, pp. 19–31.
12. P.J. Meschter, Met. Trans., vol. 23A, (1992).
13. T.C. Chou and T.G. Nieh, J. Mater. Res., vol 8, no. 1, 1993, pp. 214–223.
14. D.A. Berztiss, R.R. Cerachiara, E.A. Gulbransen, F.S. Pettit and G.H. Meier., Mater. Sci. Eng., A155. (1992), pp. 165–181.
15. A. Muller, G. Wang, R.A.Rapp, High Temperature Silicides, Eds A.K. Vasudevan, J.J. Petrovic, North Holland, Amsterdam, London, New York, 1992, pp. 199–209.
16. S.V. Raj, Mat. Sci. Eng., A201, 1995, pp. 229–241.
17. M.G. Hebsur, Intermetallic Composites III, Ed. By J.A. Graves, R.R. Bowman, and

- J.J. Lewandowski, MRS Proc. vol. 350, 1994, Pittsburgh, PA., pp. 177–182.
18. M.G. Hebsur, "Pest resistant MoSi<sub>2</sub> materials and method of making" U.S. Patent, #5,429,997, 1995.
  19. J.W. Pickens, NASA TM–102060, 44135, 1989, NASA LeRC, Cleveland, OH.
  20. M.V. Nathal and L.J. Ebert, *Metall. Trans.*, 16A, (1985), pp. 427–439.
  21. I.J. Blum, *Eng. Fract. Mech.*, (1975), pp. 593–604.
  22. A. Ghosh, M.G. Jenkins, M.K. Ferber, J. Peussa and J.A. Salem, Eds R.C. Bradt et al., Plenum Press, New York, 1992.
  23. A.J. Pyzik and D.R. Beaman, *J. Am. Ceram. Soc.*, 76, pp. 2737–2744 (1993).
  24. S. Choi and M.G. Hebsur, *American Ceramic Society Proceedings*. Jan. 1998.
  25. J.E. Ritter, in *Fracture Mechanics of Ceramics*, vol. 4, Edited by R.C. Bradt, D.P.H. Hasselman, and F.F. Lange, Plenum Publishing Corp., NY, 1978, pp. 661–686.
  26. ASTM C 1368-97 "Standard Test Method for Determination of Slow Crack Growth Parameters of Advanced Ceramics by Constant Stress-Rate Flexural Testing at Ambient Temperature," *Annual Book of ASTM Standards*, vol. 15.01, ASTM, West Conshohocken, PA, 1998 (in print).
  27. G.D. Quinn and J.B. Quinn, in *Fracture Mechanics of Ceramics*, vol. 6, Edited by R.C. Bradt, A.G. Evans, D.P.H. Hasselman, and F.F. Lange. Plenum Publishing Corp., NY, 1983, pp. 603–636.
  28. J.I. Eldridge, R.T. Bhatt and J.D. Kaiser, NASA TM–103739, 1991, NASA LeRC Cleveland OH.
  29. M.G. Hebsur and R.V. Miner, NASA TM–88950, 1987. NASA LeRC Cleveland OH.
  30. R.T. Bhatt., NASA CP–10039, 1989, pp. 57–1 to 57–13 NASA LeRC Cleveland OH.
  31. J. Halada, 'Enhanced SiC/SiC Ceramic Matrix Composites for long life performance in oxidizing environments', Du-Pont Lanxide Composites Report January 1994.
  32. P.K. Wright, *Structural Intermetallics*, Eds. R. Darolia, J.J. Lewandowski, C.T. Liu, D.B. Miracle, and M.V. Nathal, TMS, Warrendale, PA, 1993, pp. 885–893.
  33. R.C. Bradt., NASA CR–165325, 1984, NASA Washington D.C.
  34. V.C. Nardone, *Met., Trans.*, vol., 23A, 1992, pp. 563–572.
  35. K.Nakano, K. Sasaki, H. Saka, M. Fujikura, and H. Ichikawa, High Temperature Ceramic-Matrix Composites II, Manufacturing and Materials Development ed. by A.G. Evans, R.N. Nasalin, 1995, pp. 215–229.
  36. D. Eng., Private Communications, 5/98.

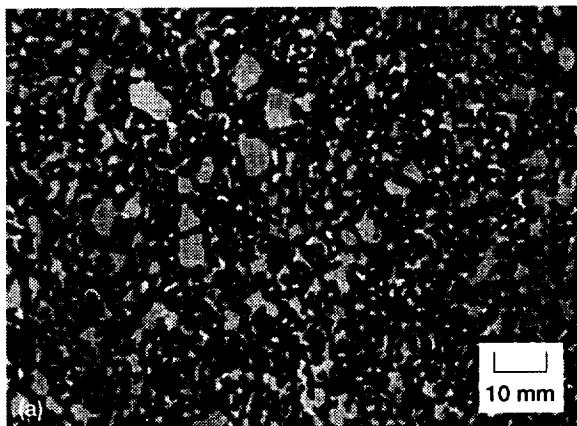


Figure 1.—(a) SEM micrograph of consolidated  $\text{MoSi}_2\text{-}50\text{Si}_3\text{N}_4$  ( $\text{MoSi}_2$  is the light phase).

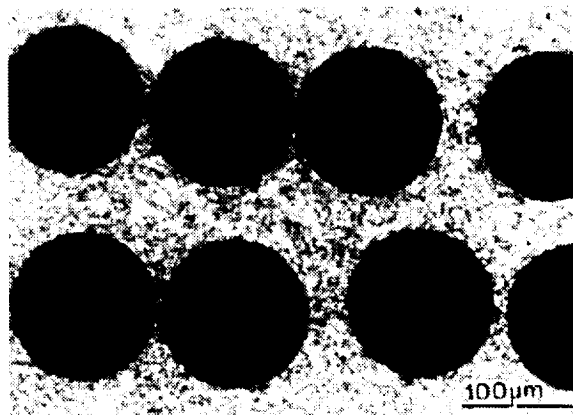


Figure 2.—SEM-back scattered image of powder cloth fabricated  $\text{SCS-6/MoSi}_2\text{-}30\text{Si}_3\text{N}_4$  hybrid.

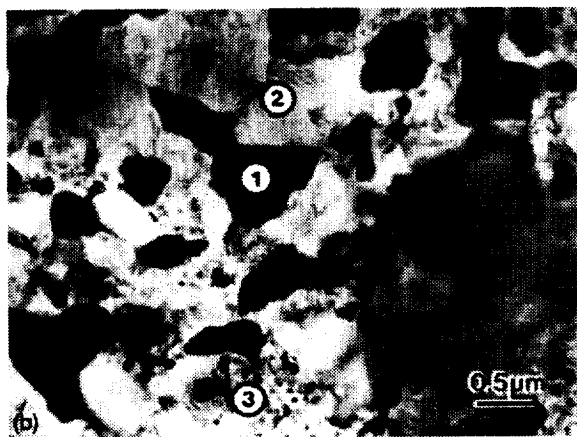


Figure 1.—(b) TEM micrograph of HP + HIP'ed  $\text{MoSi}_2\text{-}50\text{Si}_3\text{N}_4$  showing (1)  $\text{MoSi}_2$  phase (2)  $\text{Si}_3\text{N}_4$  phase, and (3) a region containing fine  $\text{Mo}_5\text{Si}_3$  phase.

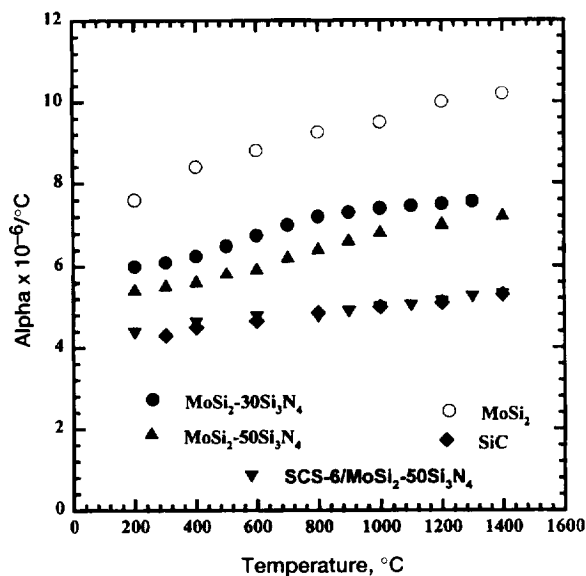
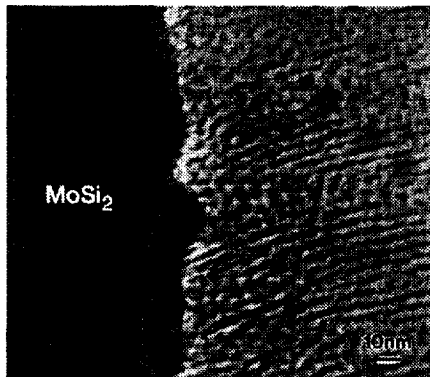
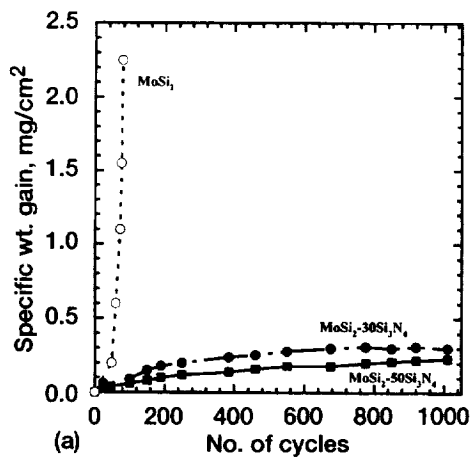


Figure 3.—Thermal expansion data for several  $\text{MoSi}_2$ -base materials and  $\text{SiC}$  reinforcing phase.



(b)

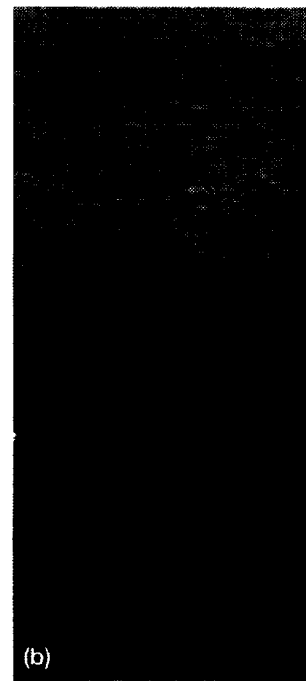


(c)

Figure 4.—Cyclic oxidation behavior of MoSi<sub>2</sub>-base materials cyclic oxidized at 500 °C in air. (a) Specific weight versus number of cycles for various MoSi<sub>2</sub>-base materials. (b) TEM micrograph of MoSi<sub>2</sub>. (c) TEM micrograph of MoSi<sub>2</sub>-30Si<sub>3</sub>N<sub>4</sub> oxidized for 1000 hours.



(a)



(b)

Figure 5 —SCS-6 fiber-reinforced specimens cyclic oxidized at 500 °C in air. (a) MoSi<sub>2</sub> matrix after 24 cycles. (b) MoSi<sub>2</sub>-30Si<sub>3</sub>N<sub>4</sub> matrix after 200 cycles.

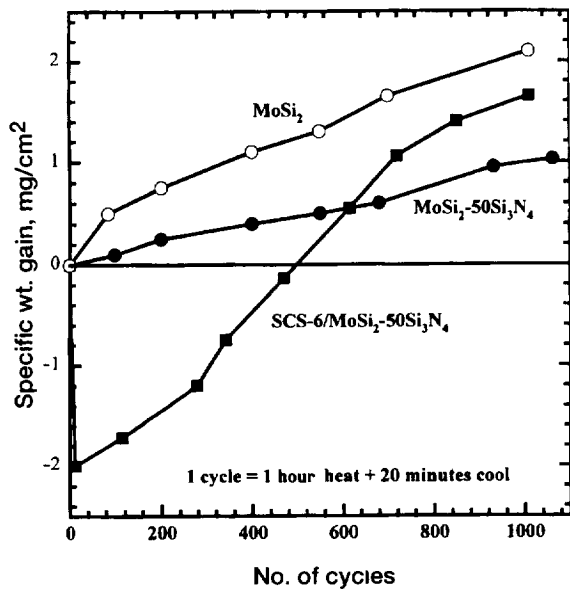


Figure 6.—Specific weight gain versus number of cycles plot for  $\text{MoSi}_2$ - $50\text{Si}_3\text{N}_4$  monolithic and  $\text{SCS-6/MoSi}_2$ - $50\text{Si}_3\text{N}_4$  hybrid composite cyclic oxidized at  $1250^\circ\text{C}$  in air.

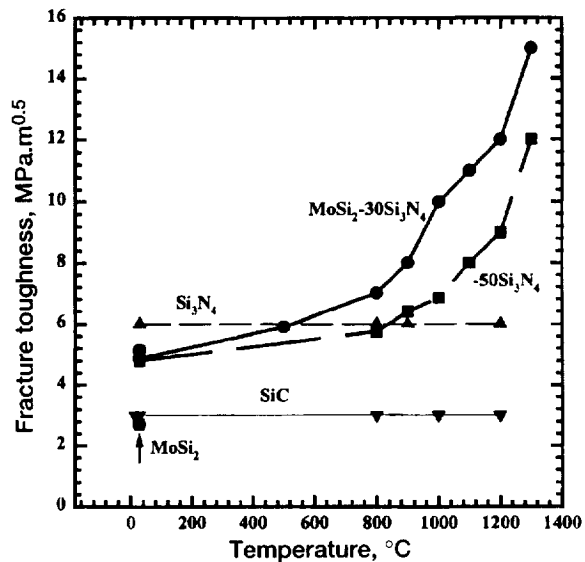


Figure 8.—(a) Temperature dependence of fracture toughness of  $\text{MoSi}_2$ -base materials compared with ceramic matrices.

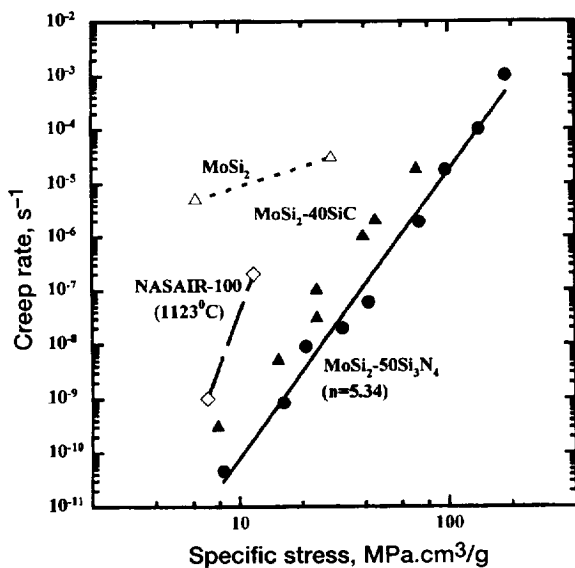


Figure 7.—Second stage creep rate versus specific stress at  $1200^\circ\text{C}$  for  $\text{MoSi}_2$ - $50\text{Si}_3\text{N}_4$  compared with other materials.

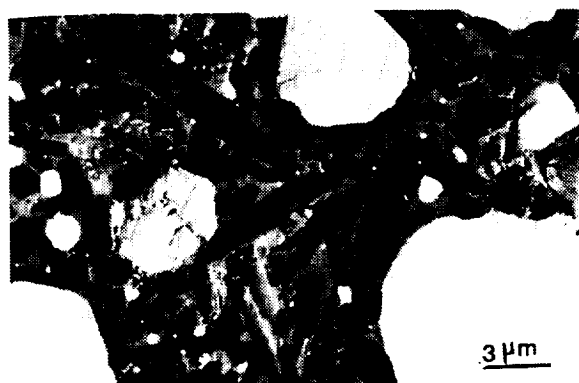


Figure 8.—(b) Field emission back scattered image of  $\text{MoSi}_2$ - $50\text{Si}_3\text{N}_4$  showing randomly oriented long whisker type grains of  $\beta\text{-Si}_3\text{N}_4$  matrix.

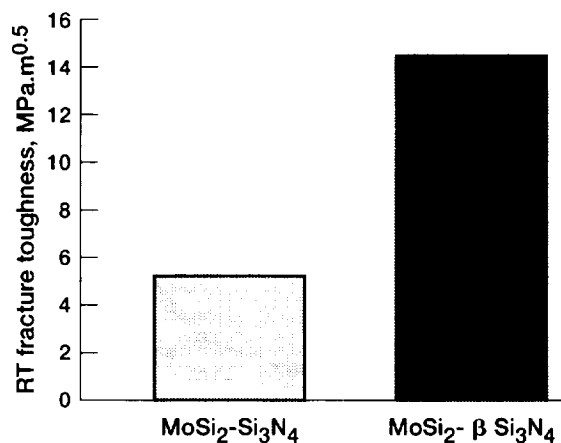


Figure 8.—(c) Nearly three times improvement in the room temperature fracture toughness of MoSi<sub>2</sub>-50Si<sub>3</sub>N<sub>4</sub> by growing whisker type β-Si<sub>3</sub>N<sub>4</sub> grains in the MoSi<sub>2</sub> matrix.

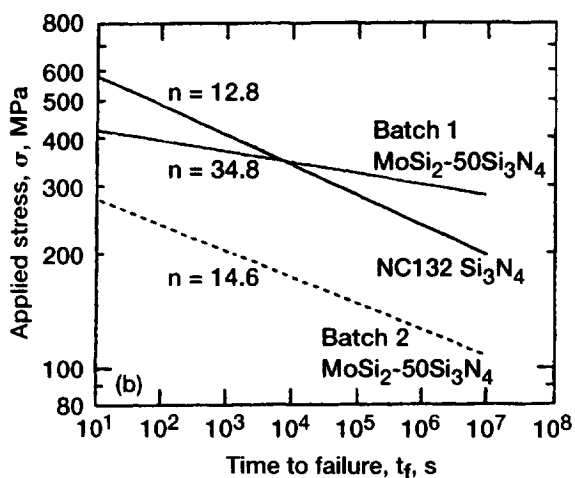
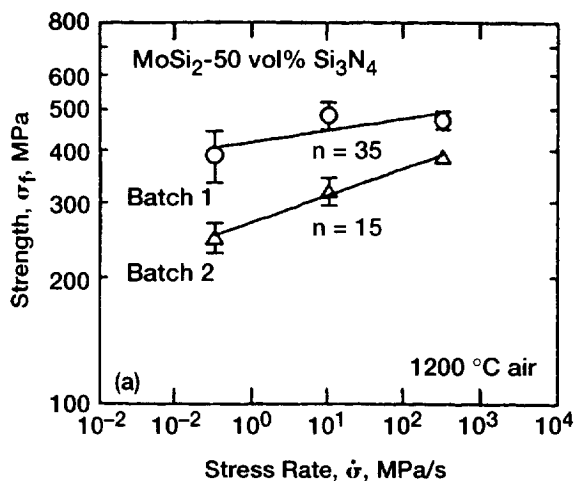


Figure 9.—Elevated temperature slow crack growth behavior of MoSi<sub>2</sub>-50Si<sub>3</sub>N<sub>4</sub>. (a) 1200 °C strength verses stress rate. (b) Life prediction diagram.

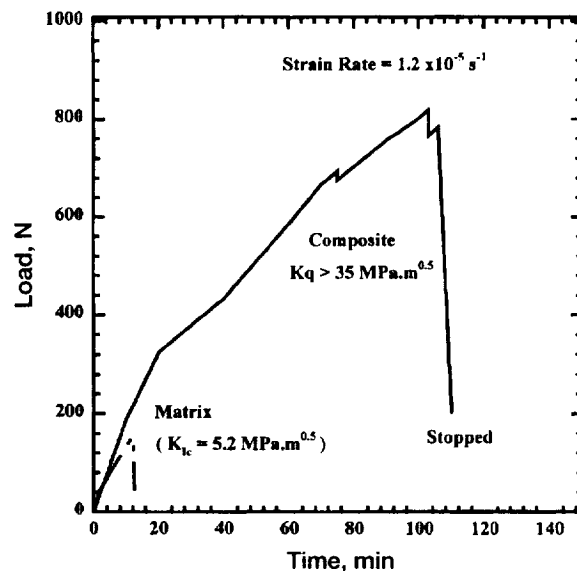


Figure 10.—Load-time curves from chevron notched 4 point bend tested SCS-6/MoSi<sub>2</sub>-50Si<sub>3</sub>N<sub>4</sub> and MoSi<sub>2</sub>-50Si<sub>3</sub>N<sub>4</sub> specimen at room temperature.

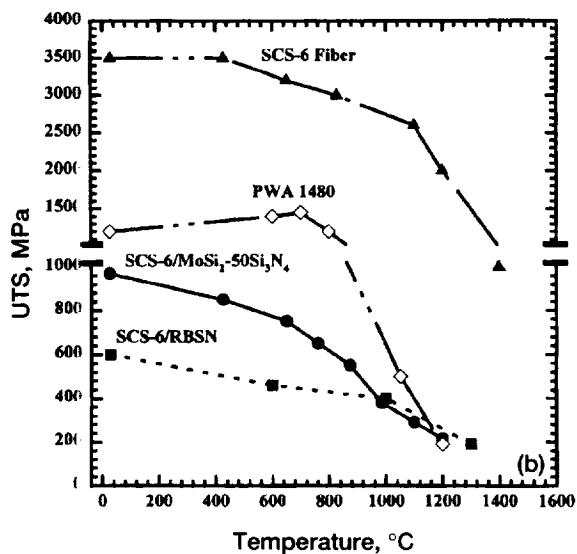


Figure 11.—(b) Temperature dependence of ultimate tensile strength of 6-ply SCS-6/MoSi<sub>2</sub>-50Si<sub>3</sub>N<sub>4</sub> base composites compared with other materials.

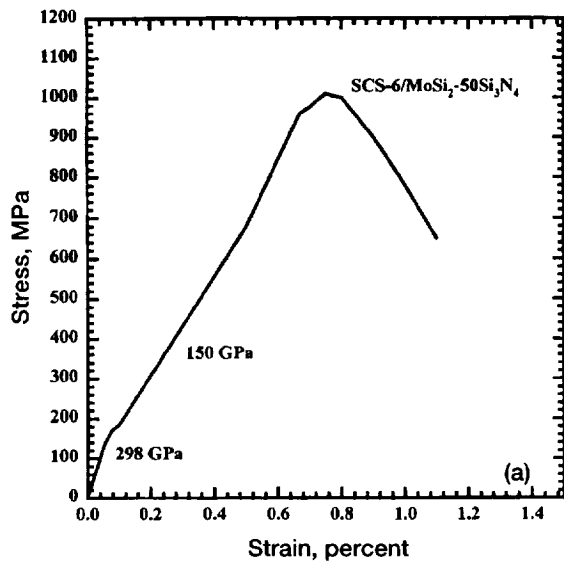


Figure 11.—(a) Room temperature tensile stress-strain curves for 6-ply SCS-6/MoSi<sub>2</sub>-Si<sub>3</sub>N<sub>4</sub> hybrid composites.

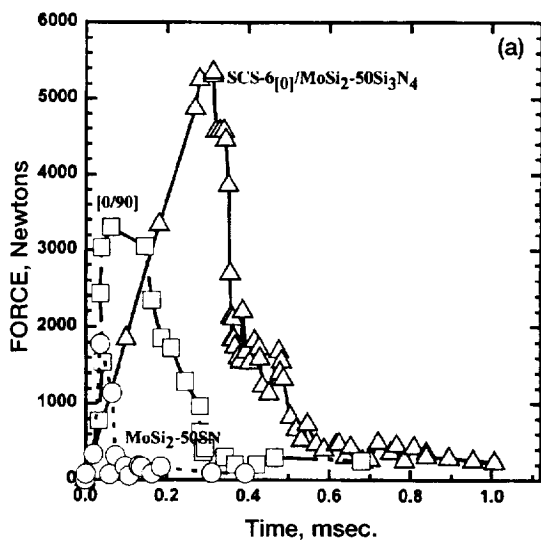


Figure 12.—(a) Force-time curves for MoSi<sub>2</sub>-Si<sub>3</sub>N<sub>4</sub> monolithic and SCS-6/MoSi<sub>2</sub>-Si<sub>3</sub>N<sub>4</sub> hybrid composites obtained from the instrumented Charpy impact tests at room temperature.

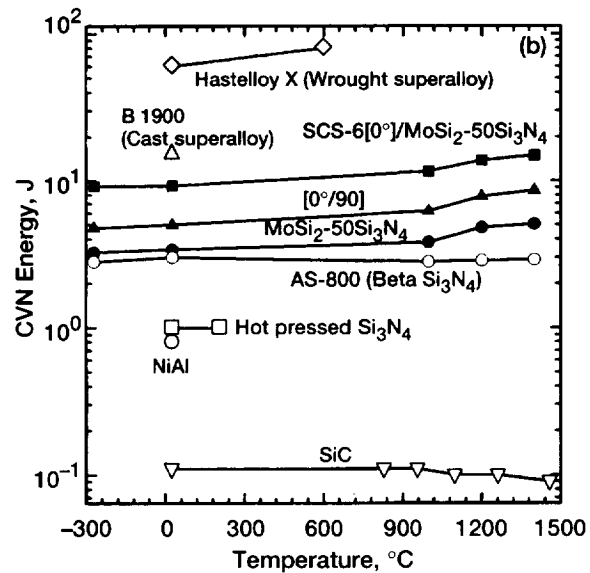


Figure 12.—(b) CVN energy versus temperature plot for MoSi<sub>2</sub>-base composites compared with other materials.

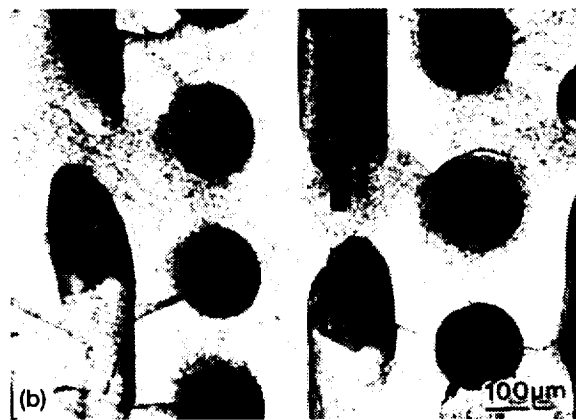


Figure 13.—SEM-BS images of impact tested SCS-6 [0°/90]/MoSi<sub>2</sub>-50Si<sub>3</sub>N<sub>4</sub> hybrid composites at (a) room temperature and (b) 1400 °C.

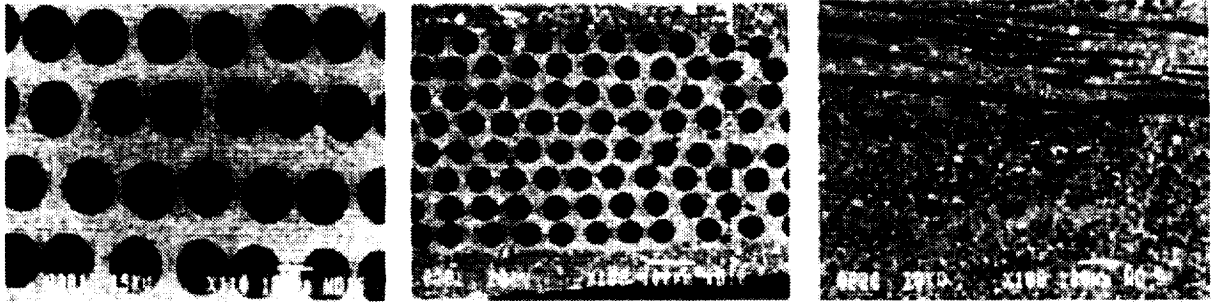


Figure 14.—SEM micrographs of SiC/MoSi<sub>2</sub>-Si<sub>3</sub>N<sub>4</sub> hybrid composites produced by two techniques and wide variety of fiber diameters. (a) Powder-cloth processed using 145 μm SCS-6. (b) Tape-cast processed using 75 μm SCS-9. (c) Tape-cast processed using 14 μm Hi-Nicalon.

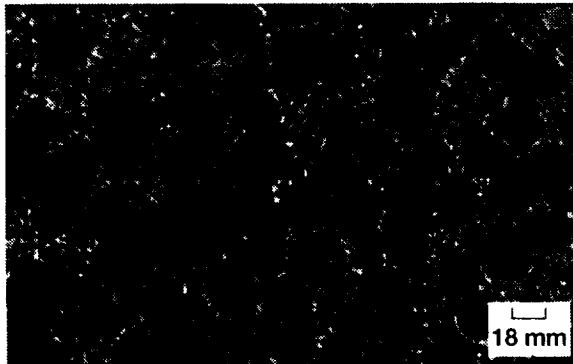


Figure 15.—SEM-SE image of BN/SiC coated Hi-Nicalon/MoSi<sub>2</sub>-Si<sub>3</sub>N<sub>4</sub> hybrid composite showing good fiber spreading and matrix infiltration.

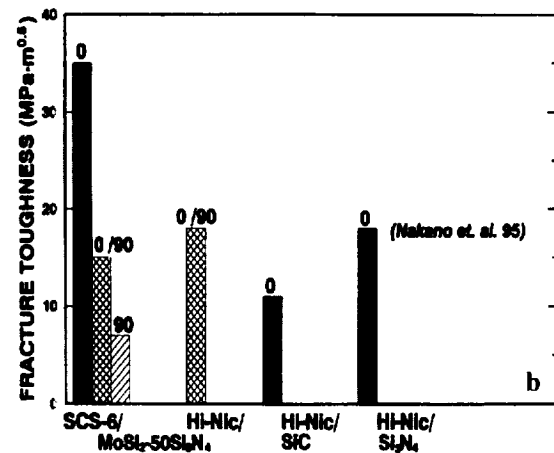
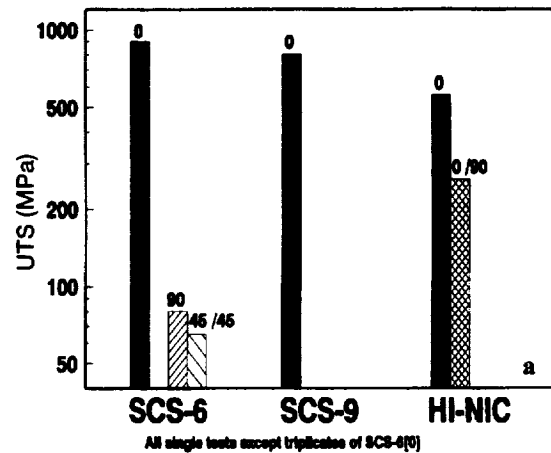


Figure 16.—Influence of fiber diameter and orientation on room-temperature (a) tensile strength and (b) fracture toughness of MoSi<sub>2</sub>-base hybrid composites.





Figure 17.—SEM-SE images of fractured toughness tested (a) BN/SiC coated Hi/Nicalon [0/90]/ (b) SCS-6 [0/90]/MoSi<sub>2</sub>-50Si<sub>3</sub>N<sub>4</sub> hybrid composites.

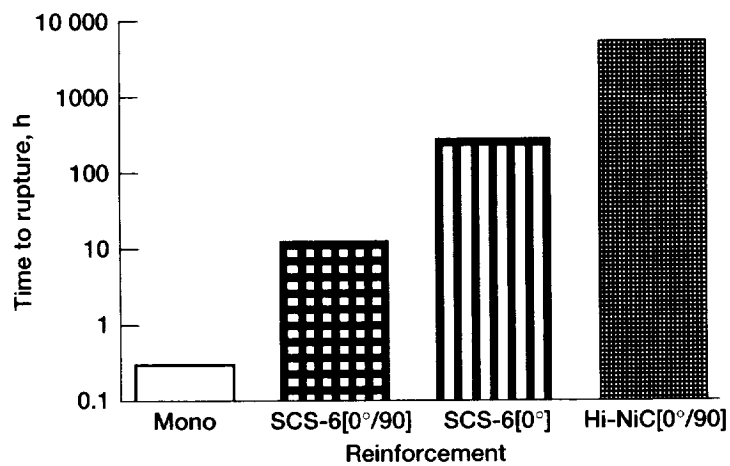


Figure 18.—Influence of SiC fiber diameter and orientation on flexural stress rupture of MoSi<sub>2</sub>-50Si<sub>3</sub>N<sub>4</sub> at 1200 °C/210 MPa.

REPORT DOCUMENTATION PAGE			Form Approved OMB No. 0704-0188	
Public reporting burden for this collection of information is estimated to average 1 hour per response, including the time for reviewing instructions, searching existing data sources, gathering and maintaining the data needed, and completing and reviewing the collection of information. Send comments regarding this burden estimate or any other aspect of this collection of information, including suggestions for reducing this burden, to Washington Headquarters Services, Directorate for Information Operations and Reports, 1215 Jefferson Davis Highway, Suite 1204, Arlington, VA 22202-4302, and to the Office of Management and Budget, Paperwork Reduction Project (0704-0188), Washington, DC 20503.				
1. AGENCY USE ONLY (Leave blank)		2. REPORT DATE October 1998		3. REPORT TYPE AND DATES COVERED Final Contractor Report
4. TITLE AND SUBTITLE  Development and Characterization of SiC/MoSi <sub>2</sub> -Si <sub>3</sub> N <sub>4(p)</sub> Hybrid Composites			5. FUNDING NUMBERS  WU-505-63-5F-00 NCC3-637	
6. AUTHOR(S)  Mohan G. Hesbur				
7. PERFORMING ORGANIZATION NAME(S) AND ADDRESS(ES)  Ohio Aerospace Institute 22800 Cedar Point Road Cleveland, Ohio 44142			8. PERFORMING ORGANIZATION REPORT NUMBER  E-11273-1	
9. SPONSORING/MONITORING AGENCY NAME(S) AND ADDRESS(ES)  National Aeronautics and Space Administration Lewis Research Center Cleveland, Ohio 44135-3191			10. SPONSORING/MONITORING AGENCY REPORT NUMBER  NASA CR-1998-208519	
11. SUPPLEMENTARY NOTES Project Manager, Michael V. Nathal, Materials Division, NASA Lewis Research Center, organization code 5160, (216) 433-9516.				
12a. DISTRIBUTION/AVAILABILITY STATEMENT  Unclassified - Unlimited Subject Category: 24 and 29  This publication is available from the NASA Center for AeroSpace Information, (301) 621-0390.			12b. DISTRIBUTION CODE	
13. ABSTRACT (Maximum 200 words)  Intermetallic compound MoSi <sub>2</sub> has long been known as a high temperature material that has excellent oxidation resistance and electrical/thermal conductivity. Also its low cost, high melting point (2023 °C), relatively low density (6.2 g/cm <sup>3</sup> versus 9 g/cm <sup>3</sup> for current engine materials), and ease of machining, make it an attractive structural material. However, the use of MoSi <sub>2</sub> has been hindered due to its poor toughness at low temperatures, poor creep resistance at high temperatures, and accelerated oxidation (also known as 'pest' oxidation) at temperatures between approximately 450 and 550 °C. Continuous fiber reinforcing is very effective means of improving both toughness and strength. Unfortunately, MoSi <sub>2</sub> has a relatively high coefficient of thermal expansion (CTE) compared to potential reinforcing fibers such as SiC. The large CTE mismatch between the fiber and the matrix resulted in severe matrix cracking during thermal cycling. Addition of about 30 to 50 vol % of Si <sub>3</sub> N <sub>4</sub> particulate to MoSi <sub>2</sub> improved resistance to low temperature accelerated oxidation by forming a Si <sub>3</sub> ON <sub>2</sub> protective scale and thereby eliminating catastrophic 'pest failure'. The Si <sub>3</sub> N <sub>4</sub> addition also improved the high temperature creep strength by nearly five orders of magnitude, doubled the room temperature toughness and significantly lowered the CTE of the MoSi <sub>2</sub> and eliminated matrix cracking in SCS-6 reinforced composites even after thermal cycling. The SCS-6 fiber reinforcement improved the room temperature fracture toughness by seven times and impact resistance by five times. The composite exhibited excellent strength and toughness improvement up to 1400 °C. More recently, tape casting was adopted as the preferred processing of MoSi <sub>2</sub> -based composites for improved fiber spacing, ability to use small diameter fibers, and for lower cost. Good strength and toughness values were also obtained with fine diameter Hi-Nicalon tow fibers. This hybrid composite remains competitive with ceramic matrix composites as a replacement for Ni-base superalloys in aircraft engine applications.				
14. SUBJECT TERMS  Intermetallic matrix; Pesting; Fracture toughness; SiC fibers; Impact; High temperature oxidation			15. NUMBER OF PAGES 29	
			16. PRICE CODE A03	
17. SECURITY CLASSIFICATION OF REPORT Unclassified	18. SECURITY CLASSIFICATION OF THIS PAGE Unclassified	19. SECURITY CLASSIFICATION OF ABSTRACT Unclassified	20. LIMITATION OF ABSTRACT	